ISBN: 978-3-95450-227-1 ISSN: 2673-5490 doi:10.18429/JACoW-IPAC2022-MOPOPT018

ADVANCING TO A GHz TRANSITION RADIATION MONITOR FOR LONGITUDINAL CHARGE DISTRIBUTION MEASUREMENTS*

S. Klaproth†[1], A. Penirschke, Thechnische Hochschule Mittelhessen, 61169 Friedberg, Germany
R. Singh, T. Reichert, GSI Helmholtzzentrum für Schwerionenforschung, 64291 Darmstadt, Germany
H. De Gersem, Technische Universität Darmstadt, 64289 Darmstadt, Germany
[1]also at Technische Universität Darmstadt, 64289 Darmstadt, Germany

Abstract

In the past, longitudinal beam profiles have been measured with e.g., Feschenko monitors, Fast Faraday Cups (FFC) and field monitors. Feschenko monitors usually examine an average shape over several pulses and FFCs are interceptive devices by design. In this work we want to present the progress in the development of a novel GHz diffraction radiation monitor which shall be able to measure the longitudinal charge distribution of single bunches within Hadron beam LINACS non-destructively. A proof-of-concept measurement has been performed at GSI. We aim for a resolution of 50 ps to 100 ps at beam energies of $\beta = 0.05$ to 0.74. electronic field simulations were performed using CST Particle Studio® to determine an optimal RF-Window, which also suits as vacuum chamber and the beam energy and angular dependencies of the diffraction radiation for different materials were analyzed.

INTRODUCTION

The longitudinal bunch shape is of interest for conditioning and verification of the beam dynamics of LINACs. While for relativistic particles pick-ups may be used to observe the longitudinal shape, non-relativistic particles self field spreads significantly along the beam axis, so that a direct correlation of the self fields and the actual charge distribution becomes ambiguous. The very same problem is given for field monitors. They also depend highly on the transverse field component which increases with the Lorentz factor γ. The response of the field monitor becomes more flattened for slower beams cause of the stretched field distribution [1].

However, there are other ways to measure the longitudinal beam profiles of non-relativistic particles like e.g., Feschenko monitors [2], which rely on beam interactions with a wire to create secondary electrons. Unfortunately, only average measurements are possible [3]. So changes of the shape from shot-to-shot measurements might not be visible. Another option to measure longitudinal beam profiles are Fast Faraday Cups (FFC). Nevertheless, those have two major disadvantages. The first is its destructive nature towards the beam itself and the second is the field elongation for non-relativistic beams, where the self field of the beam interacts with the FFC before the beam actually hits the FFC. Meanwhile, there are designs to reduce the effect of the self field [4–6], but careful handling of secondary electrons is still necessary for a longitudinal charge profile measurement.

In the following sections we will discuss the next step on advancing to a novel longitudinal beam shape monitor based on diffraction radiation. The diffraction radiation of the beam passing an aperture from the outside of the beam pipe, it is essential that the diffraction radiation can exit the vacuum system through the vacuum chamber. Hence, selecting a well-suited material is crucial for the operation of this type of monitor. The presented effect of different materials on the diffraction radiation is examined with the particle in cell solver of the simulation software CST Particle Studio®.

THEORY

A summary of the theory of the normal incident radiation (NIR) and the angular distribution of the radiated electric field [3] is given, before discussing the results of the simulation.

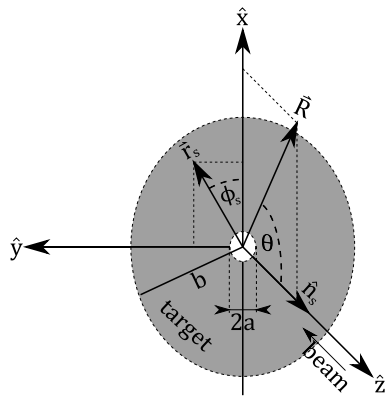

Figure 1: Coordinate system and target plane [3].

Figure 1 shows the idealized setup for the diffraction radiation simulations. The perpendicular incident bunch is passing through the aperture of radius a of the perfect electric conducting (PEC) target of radius b with velocity $\vec{v}_e = -\beta c_0 \hat{e}_z$. If the field monitor, located at $\vec{R}$, is in the x-z plane, then it should be sensitive to the emitted radiation of the field components E_x and E_z. Meaning that the relevant signal components would be $k_x \hat{e}_x + k_z \hat{e}_z$, which are generated at the surface location $\vec{r}_s$ on the target plane [3]. The angle ϕ_s describes a rotation in the target plane and θ the angle between beam axis and the position vector of the field monitor.

* This work is supported by the German Federal Ministry of Education and Research (BMBF) under contract no. 05P21RORB2. Joint Project 05P2021 - R&D Accelerator (DIAGNOSE)
† Stephan.Klaproth@iem.thm.de

ISBN: 978-3-95450-227-1 ISSN: 2673-5490 doi:10.18429/JACoW-IPAC2022-MOPOPT018

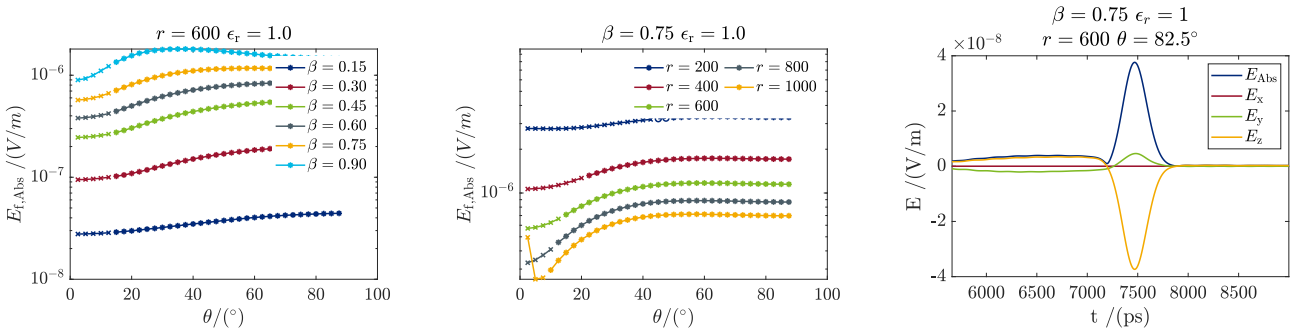

(a) (b) (c)

Figure 2: Comparison of angular field distribution E_f using FFT(E_{abs}) as NIR for (a) different beam energies and (b) different distances and (c) time domain snapshot at $\beta = 0.75$.

We follow the argumentation of [7] to obtain Eq. (1) for the special case of NIR generated at the surface of the target and observed at a field monitor. The radiation itself originates from a virtual magnetic surface current relying only on the transversal field components $E_{x,y}$ of the particles [7], so that the temporal signal corresponds to the longitudinal charge distribution.

$$\vec{E} = \frac{2e}{4\pi^2\epsilon_0\beta^2\gamma c\lambda}\int_a^b dr_s \int_0^\pi d\tilde{\phi}_s K_1\left(\frac{2\pi r_s}{\beta\gamma\lambda}r_s\right)\cos\tilde{\phi}_s \times \frac{e^{ik\tilde{R}_s}}{\tilde{R}_s^3}(1-ik\tilde{R}_s)\begin{pmatrix} z \\ 0 \\ -x - r_s\cos\tilde{\phi}_s \end{pmatrix}, \tag{1}$$

where $\tilde{R}_s$ is the shifted norm of $R_s = \|\vec{R} - \vec{r}_s\|$ using $\tilde{\phi}_s = \phi_s - \pi$, the modified Bessel's function of second kind K_1 and the corresponding wavelength λ of the generated radiation.

To evaluate the angular distribution of the radiated electric field we use the weighted sum of the frequency spectrum measured at an angle θ in distance R with respect to the target plane as given in Eq. (2) [3]

$$E_f(\theta, R) = \frac{\sum_{f=1}^{N} W_f \cdot \mathrm{NIR}(\theta, R, f)}{\sum_{f=1}^{N} W_f}, \tag{2}$$

where NIR may be replaced by the Fourier Transform of Eq. (1) or of a signal of a broad band monitor of a simulation. We weight the frequencies with the Fourier Transform of a Gaussian pulse with $W_f = \mathrm{DFT}\left[\exp\left(\frac{-t^2}{2\sigma}\right)\right]$ with $\sigma = 100$ ps. The correlation between the theoretical NIR and the CST simulations is strong [3]. Therefore, we focus only on the CST simulations. In addition, we cut the signal of the electrical field monitors, so that we only process the signal which arrives later than the particles travel time to the target plus the signal travel time to the probe. This is used to reduce the influence of the entrance radiation [3] and the diffraction radiation that occurs at the end of the shielding tube around the particle source.

As seen in Fig. 2a, the overall signal strength increases significantly with the beam energy, while the angular distribution remains similar. The distance between field monitor and target scales with $\frac{1}{R}$ [3] and drops faster at greater distances for $\theta < 40°$ (see Fig. 2b). The jump at 2.5° for distance $r = 1000$ mm is caused by mirror charges accumulated on the shielding pipe of the source leading to a constantly higher field at that location and hence to a higher E_f. An example of the time dependent signal in the y-z plane is given in Figure 2c. E_x is almost zero and only the components E_y and E_z contribute to the absolute field E_{abs} used to calculate E_f.

Table 1: Examples of Possible Vacuum Chamber Materials

Material	ϵ_r	
Alumina (99.5)	9.7 to 9.9 @1.0 MHz	[8–10]
PEEK700	6.55 to 7.25 @2.4 GHz	[10–12]
PTFE	2.1 @2.4 GHz	[10]
Quarz (Fused)	3.74 @2.4 MHz	[10, 13]

The influence of the vacuum system, especially the vacuum chamber, has not been taken into account for the time being. In Table 1 there is a selection of possible dielectric materials usable as vacuum chamber. While they all have $\mu_r = 1$ they differ in ϵ_r from 2.1 to 9.9. There will be reflections at the vacuum chamber walls due to the different ϵ_r compared to vacuum. These reflections will propagate through the vacuum chamber creating additional diffraction radiation like peaks. The signal transition through the vacuum chamber is reduced by the amount of the reflected part. Hence, the signal detection becomes difficult due to the signal-to-noise ratio as well as the correct peak selection.

PARTICLE IN CELL SIMULATION

The simulation has been simplified to investigate only the influence of the vacuum chamber's ϵ_r by using only a cylindrical vacuum chamber directly attached to the target without any sealing parts. To suppress the entry radiation [3] we use a round pipe with an inner diameter of 25 mm and a length of 140 mm. The target is a 5 mm thick PEC plate with

ISBN: 978-3-95450-227-1 ISSN: 2673-5490 doi:10.18429/JACoW-IPAC2022-MOPOPT018

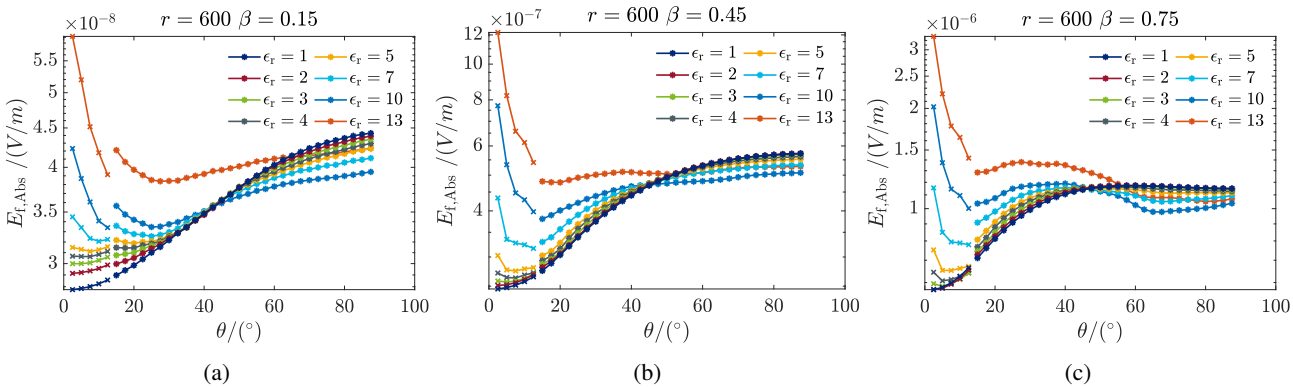

Figure 3: Comparison of angular field distribution E_f at $r = 600$ mm for (a) $\beta = 0.15$, (b) $\beta = 0.45$ and (c) $\beta = 0.75$ using FFT(E_{abs}) as NIR for different beam energies and different ϵ_r at 600 mm distance. A '×' indicates an electric field monitor inside and '∗' outside the vacuum chamber.

an aperture of $\emptyset = 40$ mm. The distance between the pipe and the target is 1 m. The vacuum chamber has a diameter of 140 mm and a thickness of 10 mm. We use a generic loss-free material varying ϵ_r and constant $\mu_r = 1$. Outside the chamber we use air as background and inside perfect vacuum. Perfect electrical monitors are positioned radially in distances of 200 mm each every 2.5° in the y-z plane. The system is excited by a $\sigma = 100$ ps Gaussian bunch with total charge of 1.6×10^{-19} C and all boundaries are set to open with an estimated reflection factor of 1×10^{-10}.

The angular field distributions E_f derived with FFT(E_{abs}) as NIR for three different β at 600 mm distance varying ϵ_r from 1 to 13 are shown in Figure 3. The symbol '×' indicates that the position of the electric field monitor is within the vacuum chamber, while a symbol '∗' says it's outside.

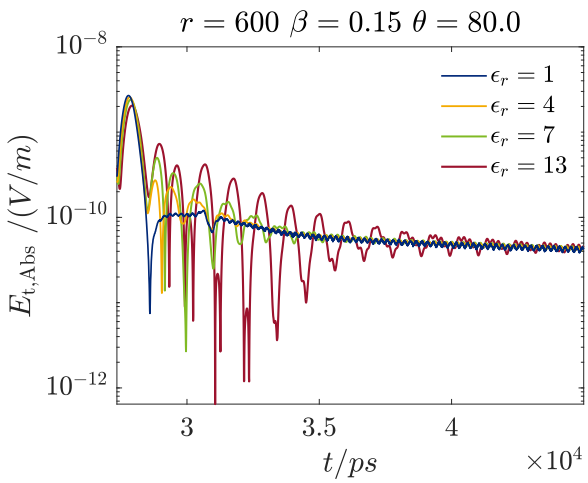

Figure 4: $E_{abs}(t)$ at $\beta = 0.15$ observed at distance $R = 600$ mm and angle $\theta = 80°$.

Within the vacuum chamber the diffraction radiation is reflected at the vacuum chamber wall. The reflection becomes more significant with increasing ϵ_r and cascades through the chamber backwards. The transitioned part of the signal is reduced accordingly to the reflected part, which becomes significantly at greater ϵ_r. The relative signal strength between the primary diffraction radiation - we want to measure - and the reflections increases with the observation angle θ. Hence, E_f is dominated by reflections for small angles - especially within the vacuum chamber - and by the primary diffraction radiation for large angles.

In Fig. 4 the time signal is shown for a selection of different ϵ_r. The reflections are clearly visible for higher permittivities. The relaxation to the undisturbed case may take 0.5 ns to 12 ns depending on ϵ_r. The amplitude of the reflections can become equally high with respect to the primary diffraction radiation depending on θ and β. The reflections lead also to the significant deformations in E_f.

CONCLUSION

In this work, the influence of material of a vacuum chamber on the expected signals at the antenna was investigated. It has been made clear that an $\epsilon_r > 5$ leads to serious reflections, which should be avoided. The detector may be placed at an angle $\theta > 40°$ and distances above $r \geq 600$ mm are beneficial concerning the reflections. The quartz fused glass chamber used in the proof-of-concept measurements [3] with an $\epsilon_r = 3.8$ [14, 15] has proven to be a good selection. Nevertheless, there are plastics with even lower ϵ_r which might be considerable like PTFE or some variants of Peek with $\epsilon_r \geq 2.6$ @2.4 GHz [11]. But especially for plastics the permeability has to be low enough, so that a pressure of $<1 \times 10^{-6}$ mbar may be reached. The simulated generic materials have been loss-free and have a constant ϵ_r for all frequencies, but real materials are lossy and generally ϵ_r is not constant for all frequencies. Also, the shape of the vacuum chamber as not been investigated. So further simulations should be done to take these into account.

ACKNOWLEDGEMENTS

This work is supported by the German Federal Ministry of Education and Research (BMBF) under contract no. 05P21RORB2. Joint Project 05P2021 - R&D Accelerator (DIAGNOSE).

ISBN: 978-3-95450-227-1 ISSN: 2673-5490 doi:10.18429/JACoW-IPAC2022-MOPOPT018

REFERENCES

[1] P. Forck, P. Kowina, and D. Liakin "Beam Position Monitors", *Synchrotron Radiat. News*, 2008, issn 1931-7344

[2] A. V. Feschenko, "Methods and Instrumentation for Bunch Shape Measurements (Invited)", in *Proc. PAC'01*, Chicago, IL, USA, Jun. 2001, paper ROAB002, pp. 517-521 vol.1.

[3] R. Singh and T. Reichert, "Longitudinal charge distribution measurement of nonrelativistic ion beams using coherent transition radiation", *Phys. Rev. Accel. Beams*, vol. 25, no. 3, p. 032801, 2022, doi:10.1103/PhysRevAccelBeams.25.032801

[4] G. Zhu, J. Wu, Z. Du, Y. Zhang, Z. Xue, H. Xie, Y. Wei, L. Jing, and H. Jia "Development of bunch shape monitor for high-intensity beam on the China ADS proton LINAC Injector II", *Rev. Sci. Instrum.*, 2018, issn 0034-6748, doi:10.1063/1.5027608

[5] J. V. Mathew and A. Bajaj, "An improved strip-line fast Faraday cup for beam bunch measurements", *Rev. Sci. Instrum.*, 2020, doi:10.1063/5.0025457

[6] A. Shemyakin, "Estimation of dilution of a Fast Faraday Cup response due to the finite particles speed", *Rev. Sci. Instrum.*, 2016, doi:10.48550/arXiv.1612.09539

[7] A. G. Shkvarunets and R. B. Fiorito, "Vector electromagnetic theory of transition and diffraction radiation with application to the measurement of longitudinal bunch size", *Phys. Rev. ST Accel. Beams*, vol. 11, no. 1, p. 012801, 2008, doi:10.1103/PhysRevSTAB.11.012801

[8] Xiamen Innovacera Advanced Materials Co., https://www.innovacera.com/materials/995-alumina

[9] Accuratus Cermaic Corporation, http://accuratus.com/pdf/995aluminaprops.pdf

[10] Material library of CST Studio Suit 2022™SP4, https://www.cst.com

[11] Preperm™ a brand of the Avient Corporation, https://www.preperm.com/products/raw-materials/#preperm-high-temperature

[12] Special Chem - The material selection platform, https://omnexus.specialchem.com/product/t-avient-formerly-polyone-preperm-peek700

[13] Heraeus Holding GmbH, https://www.heraeus.com/en/hca/fused_silica_quartz_knowledge_base_1/properties_1/properties_hca.html#tabs-608478-8

[14] EVAC AG, EVAC ISO Tapered™ adapter, pp 70, https://evacvacuum.com/wp-content/uploads/2020/02/Evac-Katalog_2020_kpl.pdf

[15] P. Sarafis and A. G. Nassiopoulou, "Dielectric properties of porous silicon for use as a substrate for the on-chip integration of millimeter-wave devices in the frequency range 140 to 210 GHz", *Nanoscale Res. Lett.*, vol. 9, no. 418, 2014, doi:10.1186/1556-276X-9-418